Pure Appl. Geophys. 174 (2017), 3331–3342

DOI 10.1007/s00024-017-1467-4

Pure and Applied Geophysics

Surface Rupture Effects on Earthquake Moment-Area Scaling Relations

Yingdi Luo,[1] Jean-Paul Ampuero,[1] Ken Miyakoshi,[2] and Kojiro Irikura[3]

Abstract—Empirical earthquake scaling relations play a central role in fundamental studies of earthquake physics and in current practice of earthquake hazard assessment, and are being refined by advances in earthquake source analysis. A scaling relation between seismic moment (M_0) and rupture area (A) currently in use for ground motion prediction in Japan features a transition regime of the form M_0–A^2, between the well-recognized small (self-similar) and very large (W-model) earthquake regimes, which has counter-intuitive attributes and uncertain theoretical underpinnings. Here, we investigate the mechanical origin of this transition regime via earthquake cycle simulations, analytical dislocation models and numerical crack models on strike-slip faults. We find that, even if stress drop is assumed constant, the properties of the transition regime are controlled by surface rupture effects, comprising an effective rupture elongation along-dip due to a mirror effect and systematic changes of the shape factor relating slip to stress drop. Based on this physical insight, we propose a simplified formula to account for these effects in M_0–A scaling relations for strike-slip earthquakes.

Key words: Earthquake scaling relations, surface rupture effects, earthquake cycle model, rate-and-state friction, analytical dislocation model, numerical crack model.

1. Introduction

Earthquake scaling relations are empirical relations between source parameters, such as seismic moment, rupture dimensions and average slip (e.g., Leonard 2010). They are significant in basic earthquake physics studies, as they constitute a first-order synthesis of static source properties to constrain earthquake mechanics models. They are also practically important as a key component of earthquake hazard assessment and ground motion prediction. Recent advances in observational techniques and source inversion methods are providing opportunities to refine the empirical relations between seismic moment and rupture geometry (Miyakoshi et al. 2015; Murotani et al. 2015) and to better understand their underlying physics.

Observations of strike-slip earthquakes show two end-member regimes in the scaling of seismic moment (M_0) vs. rupture area (A): M_0–$A^{3/2}$ for small earthquakes and M_0–A for very large ones. Intuitively, the transition between these two regimes should be M_0–A^n with an exponent n taking intermediate values, $1 < n < 3/2$. However, some authors have proposed values of n larger than 3/2. In particular, Irikura and Miyake (2011) introduced a M_0 vs. A scaling relation with three scaling regimes (referred to hereafter as Stages 1, 2 and 3, in increasing order of M_0) and $n = 2$ at intermediate magnitudes (see also, Matsu'ura and Sato 1997; Fujii and Matsu'ura 2000; Irikura and Miyake 2001; Hanks and Bakun 2002; Murotani et al. 2015). Figure 1 shows the current version of the 3-stage scaling relation calibrated by Murotani et al. (2015). In contrast to previous studies that suffer from significant uncertainties on the rupture area (e.g., Wells and Coppersmith 1994), the work of Irikura and Miyake (2011) and follow-up work are primarily based on rupture areas derived from kinematic source inversions (Somerville et al. 1999; Song et al. 2008; Miyakoshi et al. 2015; Murotani et al. 2015)(Green circles in Figure 1 shows observational data from kinematic inversion of vertical strike-slip faults (Somerville et al. 1999; Miyakoshi et al. 2015; Murotani et al. 2015)). While the empirical data strongly supports Stage 1, evidence for Stage 3 has been the subject of a long-standing debate due to the limited number of very large strike-slip earthquakes (Scholz 1982; Romanowicz and Rundle 1993, etc.).

[1] Seismological Laboratory, California Institute of Technology, Pasadena, CA, USA. E-mail: luoyd@gps.caltech.edu
[2] Geo-Research Institute (GRI), Osaka, Japan.
[3] Aichi Institute of Technology (AIT), Toyota, Japan.

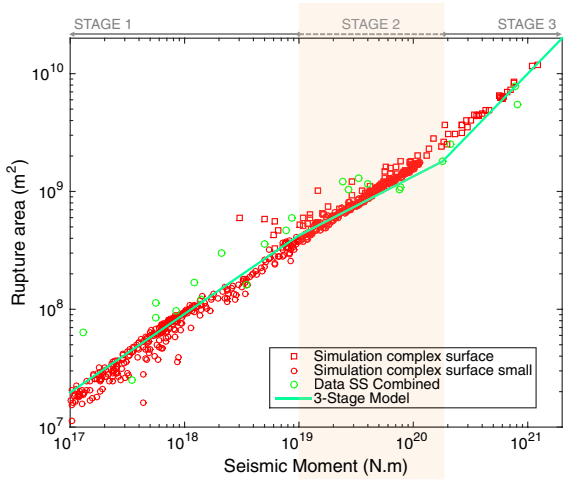

Figure 1
Earthquake seismic moment (M_0) vs. rupture area (A) empirical and simulation data and 3-stage scaling model. *Green curve*: empirical 3-stage relation by Murotani et al. (2015). *Green circles* observational data from kinematic inversion of vertical strike-slip faults (Somerville et al. 1999; Miyakoshi et al. 2015; Murotani et al. 2015). *Red circles and squares* synthetic earthquake data from our rate-and-state simulation of "reduced-scale" and "full-scale" models, respectively

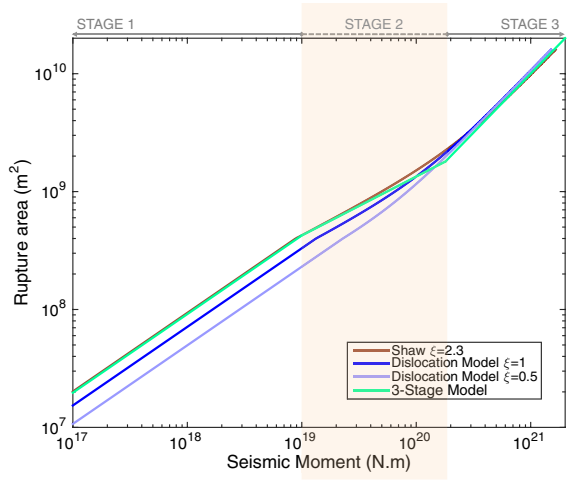

Figure 2
Earthquake M_0–A relations for dislocation and deep rupture penetration models. *Brown curve* deep penetration model (Shaw and Wesnousky 2008, Shaw 2009). *Dark blue curve* our dislocation model with free surface (Model D2, $\xi = 1$). *Light blue curve*: our dislocation model without free surface (Model D1, $\xi = 0.5$). *Green curve* empirical 3-Stage relation by Murotani et al. (2015). Model D2 has Stage 2 while model D1 does not, which indicates that the free surface is key to Stage 2

Irikura and Miyake (2001) and Hanks and Bakun (2002) independently proposed Stage 2, Murotani et al. (2015) calibrated its properties based on slip distributions inferred by source inversion, and Miyakoshi et al. (2015) analyzed a large number of crustal earthquakes in Japan to confirm the existence of Stage 2. Our focus here on the 3-stage scaling relation introduced by Irikura and Miyake (2011) and calibrated by Murotani et al. (2015) is motivated by its wide adoption in ground motion prediction studies in Japan. The study of the 3-stage model, especially the least understood Stage 2, is of great importance in earthquake hazard estimation because the seismic moment predicted for a given rupture area, and hence strong ground motions, can be significantly higher if predictions include Stage 2.

The present work aims at developing a mechanical model consistent with Stage 2, namely $M_0 \sim A^2$ for $10^{19} < M_0 < 1.8 \times 10^{20}$ N m or moment magnitude Mw 6.6 to 7.5 (Murotani et al. 2015). Stage 1 is classically explained by a self-similar rupture model, e.g., a circular crack with scale-independent stress drop. Stage 3 is naturally explained by the so-called W-model, a rupture very elongated along-strike with scale-independent depth extent and stress drop (Scholz 1982; Bodin and Brune 1996; Mai and Beroza 2000; Leonard 2010). Due to the limited number of available observations of very large strike-slip earthquakes, other models like the L-model have also been advocated (Hanks and Bakun 2002). Three main models have been proposed to explain Stage 2: rupture penetration below the seismogenic zone (Shaw and Wesnousky 2008, Shaw 2009), effect of the viscous asthenosphere (Matsu'ura and Sato 1997), and scale-dependent stress drop (Dalguer et al. 2008). On the one hand, evidence for the deep rupture penetration required by Shaw's model (up to 46 km depth in Fig. 2) and for scale-dependent stress drop are scarce (e.g., Hanks and Bakun 2014). On the other hand, the model by Matsu'ura and Sato (1997) assumes that the depth of the lithosphere and the depth of the seismogenic zone are the same, which is inconsistent with the current view that faults slip aseismically in the lower crust. Hence, the mechanical origin of Stage 2 remains unclear.

In this study, we develop a mechanical model consistent with the 3-stage M_0–A scaling relation of Murotani et al. (2015). We show that the existence of

Stage 2 can be attributed to surface rupture effects, even if stress drop is constant. Thus the effects of scale-dependent stress drop, deep rupture penetration and deeper viscous rheology, while possibly present, can be considered as secondary. In Sect. 2 we present results of rate-and-state earthquake cycle simulations with a wide magnitude range that are consistent with the observational data and the 3-stage scaling relation. In Sect. 3 we investigate dislocation models and find a geometrical effect of the free surface that contributes to Stage 2. In Sect. 4 we develop crack models that fit the proposed 3-stage model and reveal a shape factor effect of the free surface that further contributes to Stage 2. Based on our numerical and analytical results, we propose a simplified equation that captures the 3-stage earthquake scaling relation.

2. A Rate-and-State Earthquake Cycle Model

We perform multi-cycle quasi-dynamic simulations on vertical strike-slip faults governed by rate-and-state friction with heterogeneous characteristic slip distance (D_c). In contrast with dynamic rupture simulations of single earthquakes, multi-cycle modeling does not require assumptions about initial stresses before each earthquake: heterogeneous stresses emerge spontaneously throughout the cycles and lead naturally to heterogeneous co-seismic slip distributions. The approach is similar to that developed in Hillers et al. (2006, 2007), where more details can be found, but progress in computational capabilities allows us to adopt realistic values of the radiation damping coefficient. Our simulations are done with the boundary element method with adaptive time-stepping implemented in the software QDYN (Luo and Ampuero, http://ydluo.github.io/qdyn/). The fault is governed by the laboratory-motivated rate-and-state friction law (Marone 1998). The friction parameter D_c is the characteristic slip distance of frictional evolution and controls the fracture energy and nucleation length (Rubin and Ampuero 2005). Two friction parameters, a and b, control the non-linear viscous resistance and slip-weakening rate of the frictional surface, respectively. Their competition leads to either velocity-weakening (VW) behavior when $a < b$, allowing earthquake nucleation, or velocity-strengthening (VS) behavior when $a > b$, promoting stable sliding (Scholz 1998). The distribution of frictional properties as a function of depth introduces VW to VS transitions at depth and near the surface controlled by the temperature dependence of a and b (Figs. 3, 4c). Our model faults have a reference seismogenic depth (W_{Sref}) of 18 km defined as the width of the VW region (from 2 to 20 km depth). On natural faults the seismogenic depth is often defined by the lower depth of the distribution of hypocenters, which corresponds to the bottom of the VW region in our model. The effective normal stress increases linearly from 0 to 10 km depth until it saturates at 75 MPa based on the assumption that pore pressure increases at the same rate as the lithostatic stress at depth (super-hydrostatic pore pressure, e.g., Streit and Cox 2001). We assume a stochastic, spatially correlated lognormal distribution of D_c. The model parameters are tuned so that each individual model produces seismic events of various magnitudes. In addition, in order to obtain events with a sufficiently wide range of magnitudes, we combine results from multiple models with different random seeds, correlation lengths L_{co} and ranges of D_c values. Typical values used in our rate-and-state simulations are provided in Table 1. Figure 3, right, shows the D_c profile of a typical model. A thorough discussion of how model parameters affect the distribution of magnitudes will be published elsewhere (see also Hillers et al. 2006, 2007). A characteristic length scale of the problem is the nucleation size $L_c = G \times D_c/((b - a)\sigma)$, where G is the shear modulus and σ is the effective normal stress. To reduce the computational cost, we combined two sets of simulations. A "full-scale" set targets Stages 2 and 3 on long faults (512 km length) with minimum and average L_c of 2.7 km and 6 km, respectively, at the middle depth of the seismogenic zone. A "reduced-scale" set targets Stages 1 and 2 on smaller faults (64 km length) with half smaller D_c and finer mesh. The nucleation size also varies between models with different D_c ranges. The range of magnitudes obtained from these two sets of simulations has significant overlap, which allows us to verify that our composite approach does not generate artifacts in the scaling relations. The seismic events detected in all these simulations are combined in a

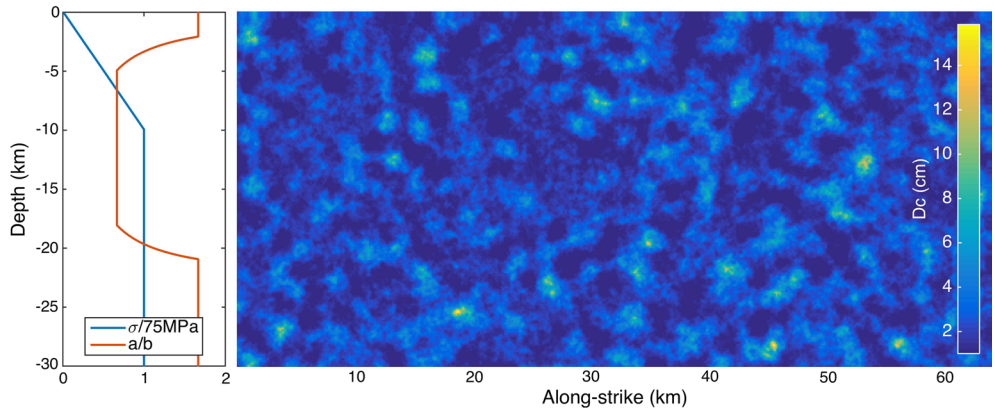

Figure 3
Rate-and-state model settings. *Left* effective normal stress (*blue curve*) and *a/b* ratio (*red curve*) as a function of depth. The seismogenic zone ($a/b < 1$) extends roughly from 2 to 20 km depth. *Right* an example of heterogeneous distribution of characteristic slip distance D_c with correlation length of 1 km

single catalog with over 10,000 events whose seismic moments span over 4 orders of magnitude.

We detect seismic events based on slip-rate thresholds. Because of significant slip-rate fluctuations caused by the strong heterogeneity of D_c, the event detection procedure artificially divides some large events into several smaller successive events. We crudely mitigate this unrealistic feature by treating events that occur less than 10 min apart as being part of the same rupture. This correction comes with the cost of possibly overlooking some very early aftershocks. However, manual inspection shows that the number of overlooked aftershocks is very limited, and our focus here is on earthquake scaling rather than individual events, hence the benefits of amendment greatly outweigh its limitations.

The small events in our simulated catalog have unrealistic, scale-dependent stress drops that may adversely affect the scaling results. Those unrealistic stress drops have two main origins. First, relatively large D_c values are used to keep the computational cost affordable, leading to large nucleation areas with large aseismic pre-slip within which co-seismic stress drops are unrealistically low. Second, our catalog still contains some ill-shaped early aftershocks which should have been considered as part of their main shock rupture. Note that only events in Stage 1 are significantly affected by these artifacts, while in Stages 2 and 3, which span over 2 orders of magnitude, stress drops show no significant scale-dependency (Fig. 5). The variability of stress drop in Stages 2 and 3 is much smaller than the variability inferred for real earthquakes: the standard deviation of $\ln \Delta\tau$ (stress drop) from our rate-and-state simulations is 0.1, while from seismological estimates it is 0.7 or more (e.g., Table 1 of Causse and Song 2015). To mitigate the stress drop artifacts and to focus on the effect of geometry and free surface on the moment-area scaling, we compute for each event in our simulated catalog the spatial average of stress drop over the rupture area (defined as the area where peak slip rate exceeds 1 cm/s), then we divide its moment by the average stress drop and multiply it by a reference stress drop $\Delta\tau_{ref}$. In the resulting modified catalog all events have the same average stress drop, $\Delta\tau_{ref}$, and the scattering in the M_0–A scaling plots is significantly reduced. While earthquake moment-area data can be alternatively interpreted as resulting from scale-dependency of stress drop (Dalguer et al. 2008), validation of this hypothesis has been challenging due to the large uncertainties of seismological estimates of stress drops. Here we will demonstrate that a model with constant stress drop is sufficient to explain the main characteristics of Stage 2.

Two model parameters are calibrated to achieve a good match of the empirical M_0–A relation: the seismogenic depth (W_s) and the stress drop ($\Delta\tau$). Dimensional analysis shows that, assuming the ratio L_c/W_s is fixed, A is proportional to W_s^2 and M_0 is proportional to $\Delta\tau W_s{}^3$ (since $M_0 = G\,A\,D \propto A\,\Delta\tau$

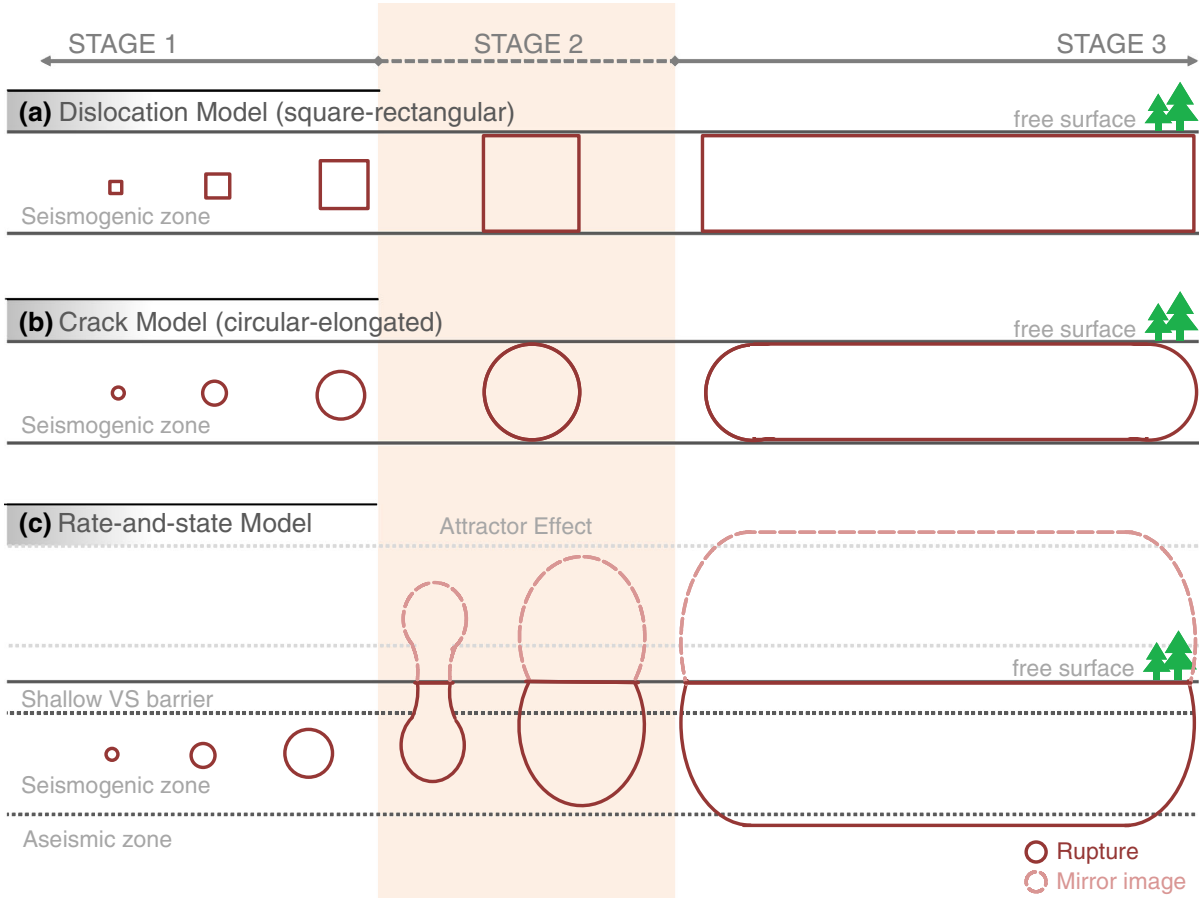

Figure 4
Rupture geometry in different models considered in this study. **a** Dislocation model with square to rectangular rupture transition. **b** Crack model with circular to elongated rupture transition. **c** Rate-and-state model with self-similar to elongated rupture transition. The free surface mirror image effect applies to all models. The 'attractor effect' (coalescence between real and mirror image ruptures) enhances Stage 2 in the rate-and-state model

$W_s \propto \Delta\tau\, W_s^3$). We can use this rationale to rescale our reference model results to obtain catalogs for different values of W_s and $\Delta\tau$. We first rescale the seismogenic depth: we multiply A by $(W_s/W_{s_{ref}})^2$ and M_0 by $(W_s/W_{s_{ref}})^3$ where the seismogenic depth W_s is tuned to match as well as possible the range of M_0 spanned by Stage 2 in the empirical model. We then rescale the stress drop: we multiply M_0 by $\Delta\tau/\Delta\tau_{ref}$, where the stress drop $\Delta\tau$ is tuned to obtain the best overall match to the empirical model. The moment and rupture area data from our simulation catalog after these post-processing steps are shown in Fig. 1. The resulting M_0–A scaling is in reasonable agreement with the 3-stage empirical relation. The events transit from small, self-similar ruptures to large, elongated ruptures (Fig. 4c), and the M_0–A scaling displays all the three stages. The best fitting model parameters have reasonable values: $W_s = 20$ km and $\Delta\tau = 2.4$ MPa. The best fitting seismogenic depth of our rate-and-state model is in the upper end of the typical range of seismogenic depths of real strike-slip faults. Penetration of rupture into the deep VS region is observed in the large events of our rate-and-state simulations (Stage 3), but remains modest, up to 2 km into the VS region (approximately 10% of seismogenic depth).

An additional set of simulations reveals the importance of the free surface in generating Stage 2.

Table 1

Typical parametric settings of rate-and-state simulation

Physical properties	Value
Total fault depth	30 km
Reference seismogenic depth	About 18 km
Total fault length	64 km/512 km ("reduced-scale"/"full-scale" fault)
Fault dipping	90° (vertical strike-slip)
Effective normal stress	0–75 MPa (saturated at 10 km)
Lamé's first parameter	30 GPa
Lamé's second parameter (shear modulus)	30 GPa
Shear wave velocity	3000 m/s
Frictional coefficient a (direct effect)	0.01
Frictional coefficient b (indirect effect)	0.015 (VW)/0.006 (VS)
Characteristic slip distance D_c	Lognormal distribution 0.01–0.15 m
D_c correlation length L_{co}	1–10 km
Reference friction coefficient	0.6
Grid size	125/250 m ("reduced-scale"/"full-scale" fault)
Post-processing parameters	**Value**
Event detecting threshold	Global max slip rate of 0.01 m/s
Event separating threshold	10 min between events
Best fitting stress drop	2.4 MPa
Best fitting seismogenic depth	20 km

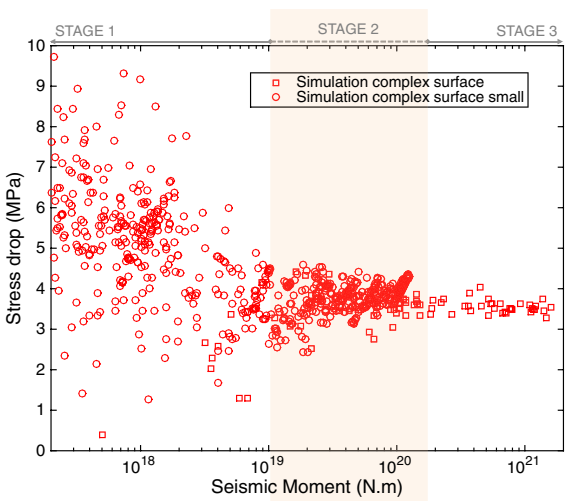

Figure 5
Stress drop as a function of seismic moment from rate-and-state simulations. *Red circles and squares* synthetic earthquake data from rate-and-state simulation of "reduced-scale" and "full-scale" models, respectively. In stages 2 and 3 the variability of stress drop is small

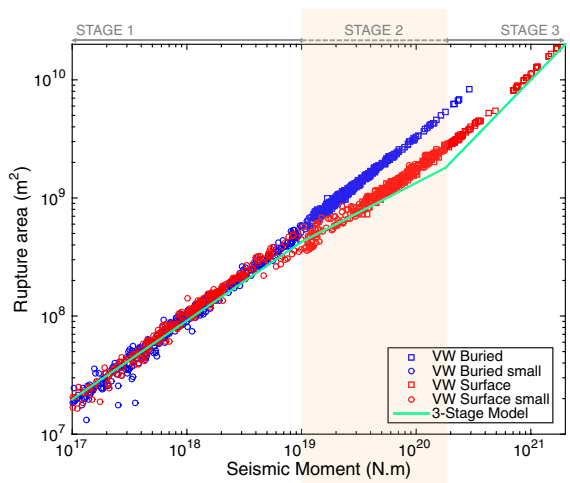

Figure 6
Effect of free surface on M_0–A scaling. *Red circles and squares* synthetic earthquake data from rate-and-state simulation with free surface in "reduced-scale" and "full-scale" models, respectively. *Blue circles and squares* synthetic earthquake data from rate-and-state simulation without free surface in "reduced-scale" and "full-scale" models, respectively. *Green curve* empirical 3-Stage relation. The difference between the two rate-and-state models indicates that the free surface is the key to Stage 2

We ran earthquake cycle simulations on a pure velocity-weakening, deeply buried fault. Other settings are comparable to those of the simulations introduced above; the main difference is the absence of the free surface in the new set. The resulting catalog shows Stages 1 and 3, but no Stage 2 (Fig. 6). In the next sections we develop a theoretical

understanding of surface rupture effects on M_0–A scaling relations.

3. Dislocation Models

We first develop a dislocation model for which we can obtain an analytical expression of the M_0–A relation in closed form, allowing fundamental insight into the problem. Dislocation models are rupture models with prescribed uniform slip and rupture geometry. The rupture shapes are assumed square for small events with rupture length $L < W_s$ and rectangular for large events with $L > W_s$ (Fig. 4a). We consider two cases: (D1) without free surface and (D2) with free surface. The latter is achieved by mirroring the rupture with respect to the free surface.

From formulas for the stress changes induced by a rectangular dislocation in unbounded media (Gallovic 2008), we derive the following relation between average slip $\bar{d}$ and stress drop $\Delta\tau$ at the center of a dislocation of length L and width W:

$$\bar{d} = \frac{\pi\overline{\Delta\tau}}{2G} \times \frac{f\left(\frac{L}{2\xi W}, \upsilon\right)}{\sqrt{1/L^2 + 1/(2\xi W)^2}}, \tag{1}$$

where

$$f(x,\upsilon) = \frac{x^2+1}{x^2 + 1/(1-\upsilon)},$$

υ is Poisson's ratio and ξ is a dimensionless parameter accounting for the free surface: $\xi = 0.5$ for a deeply buried dislocation (D1) and $\xi = 1$ for a vertical strike-slip dislocation breaking the free surface (D2). The seismic moment is

$$M_0 = GA\bar{d}. \tag{2}$$

For ruptures smaller than the seismogenic depth W_s we assume self-similarity, $L = W$, and the rupture area is $A = L^2$. For longer ruptures that saturate the seismogenic depth, $L > W = W_s$ and $A = LW_s$. Combining Eqs. (1) and (2) gives in these two cases:

$$M_0 = L^3 \times \frac{\pi\overline{\Delta\tau}}{2} \times \frac{f\left(\frac{1}{2\xi}, \upsilon\right)}{\sqrt{1 + \left(\frac{1}{2\xi}\right)^2}} \quad L \le W_s, \tag{3a}$$

$$M_0 = LW_s \times \frac{\pi\overline{\Delta\tau}}{2} \times \frac{f\left(\frac{L}{2\xi W_s}, \upsilon\right)}{\sqrt{\left(\frac{1}{L}\right)^2 + \left(\frac{1}{2\xi W_s}\right)^2}} \quad L > W_s. \tag{3b}$$

From this we derive the following moment-area relations:

$$M_0 = A^{3/2} \times \frac{\pi\overline{\Delta\tau}}{2} \times \frac{f\left(\frac{1}{2\xi}, \upsilon\right)}{\sqrt{1 + \left(\frac{1}{2\xi}\right)^2}} \quad L \le W_s, \tag{4a}$$

$$M_0 = A \times \frac{\pi\overline{\Delta\tau}}{2} \times \frac{f\left(\frac{A}{2\xi W_s^2}, \upsilon\right)}{\sqrt{\left(\frac{W_s}{A}\right)^2 + \left(\frac{1}{2\xi W_s}\right)^2}} \quad L > W_s. \tag{4b}$$

Equation (4a) shows that the dislocation model reproduces the M_0–$A^{3/2}$ scaling of Stage 1 when $L < W_s$. By considering the asymptotic behavior of Eq. (4b) we find that the dislocation model also reproduces the M_0–A scaling of Stage 3 when $L \gg W_s$. The resulting M_0–A curves, shown in Fig. 2 (assuming $W_s = 20$ km, $\Delta\tau = 3$ MPa for model D1 and $\Delta\tau = 1.5$ MPa for model D2), confirm that both models have Stages 1 and 3. However, only model D2 has a noticeable Stage 2, which appears in Fig. 2 as an intermediate regime with lower slope than Stages 1 and 3. This confirms our previous conclusion that the free surface is essential for Stage 2.

In model D2, because of our simplified use of the mirror image method, the stress drop is actually evaluated at the surface rather than at mid-rupture depth. Evaluating it a mid-depth yields a more complicated formula and a M_0–A relation in between models D1 and D2.

An asymptotic argument provides insight on the role of the free surface. By extrapolating Eq. (4b) towards $L \ll W_s$ ($A \ll W_s^2$), essentially considering ruptures that are elongated in the vertical direction, yields:

$$M_0 = \frac{A^2}{W_s} \times \frac{\pi\overline{\Delta\tau}}{2} \times (1-\upsilon). \tag{5}$$

This is a $M_0 \sim A^2$ relation like the proposed Stage 2. Hence, the dislocation model reveals an underlying asymptotic tendency towards Stage 2 due

to vertical elongation of the rupture. The vertical elongation is not necessarily real: an effective elongation may result from the free surface effect. In an infinite space model, the free surface can be mimicked by a mirror image rupture. The effective rupture (the combination of real and image ruptures) is elongated vertically up to an aspect ratio of 2. This is a geometrical effect of the free surface, which we denote as the 'G effect'.

Our rate-and state simulations reveal an additional 'surface attraction effect' that enhances the G effect. The shallow VS zone discourages small events from breaking the surface. Ruptures that grow to a certain size (still smaller than W_s) penetrate the shallow VS barrier and may break the free surface. Considering the free surface as a mirror, the real and image ruptures are two interacting coplanar cracks. The stress increase beyond their tips enhances their propagation, they attract each other and coalesce. This attractor effect can extend the vertical elongation beyond aspect ratio of 2, thus further enhancing the 'G effect' (Fig. 4c).

The dislocation model D2 agrees qualitatively with our rate-and-state model (Fig. 7). However, it cannot fit the empirical Stages 1 and 3 simultaneously: the width of Stage 2 is narrower than in the empirical model. This limitation of dislocation models motivates our next improvement of the theory.

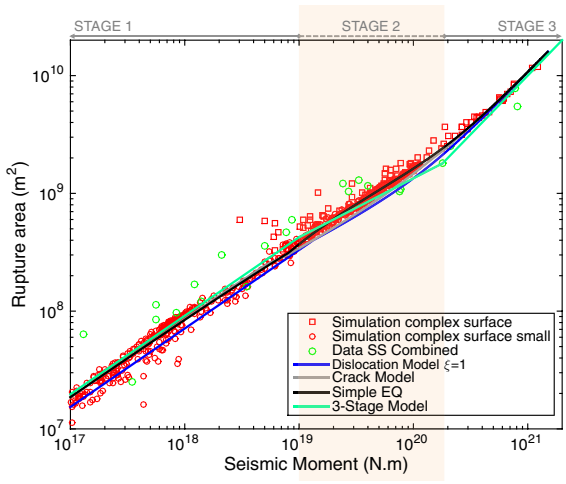

Figure 7
Earthquake M_0–A scaling in empirical data, synthetic catalogs and theoretical models. *Green circles* strike-slip earthquake data (from kinematic inversion of vertical strike-slip faults (Somerville et al. 1999; Miyakoshi et al. 2015; Murotani et al. 2015)). *Green curve* empirical 3-stage relation. *Red circles and squares* synthetic earthquake data from earthquake cycle simulations of "reduced-scale" and "full-scale" models, respectively. *Dark blue curve* dislocation model with free surface (Model D1). *Grey curve* crack model. *Black curve* proposed simple Eq. (8) with best fitting parameters $p = 2.08$ and $\lambda = 1.93$. The crack model fits the data better than the dislocation model, and the simple Eq. (8) fits both the simulation and observation data extremely well

4. Crack Models

We now consider crack models, i.e., models in which stress drop is prescribed within a given rupture area. There is no simple analytical M_0–A expression for a crack of general shape and including the free surface, so we compute it numerically. The spatial distributions of slip and stress drop, discretized over a fault grid, are related by a linear system of equations whose coefficients can be computed with formulas by Okada (1992). We prescribe a rupture geometry and uniform stress drop ($\Delta\tau$), and solve the system of equations to obtain the slip distribution. We then compute the average slip $\bar{d}$ and the "geometrical shape factor" C defined by

$$C = \Delta\tau \min(L, W_s)/G\bar{d}, \tag{6}$$

C is a non-dimensional function of L/W_s. Knowing C we can calculate M_0 of any given event using

$$M_0 = GA\bar{d} = \Delta\tau \min(L, W_s)A/C. \tag{7}$$

We solved crack models ranging from small circular ruptures (100 m in diameter) to horizontally elongated ruptures (up to 600 km in length). The latter have semi-circular lobes on both lateral ends (Fig. 4b) to ensure a smooth shape transition from circular to elongated ruptures. We have considered other shapes of crack models but the presented model offers the best fit to data.

The M_0–A curve resulting from the crack model is shown in grey in Fig. 7. This model also reproduces the 3 stages. Overall, it fits better the empirical relation than our dislocation models: it can fit Stages 1 and 3 simultaneously and has a reasonable range of Stage 2. The crack model also agrees well with our rate-and-state model.

Our crack model reveals an additional mechanism contributing to Stage 2: the change of shape factor

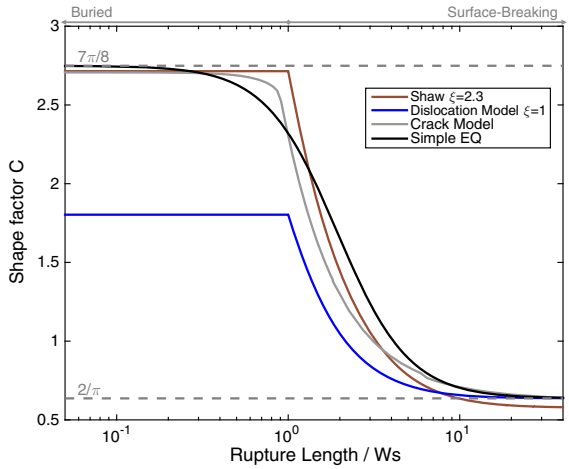

Figure 8
Shape factor C of different models as a function of rupture length L normalized by seismogenic depth W_s. *Brown curve* Shaw's deep penetration model. *Blue curve* dislocation model with free surface (model D2). *Grey curve* crack model with free surface. *Black curve* our proposed simple Eq. (8) with best fitting parameters $p = 2.08$ and $\lambda = 1.93$. The theoretical values of an infinitely long strike-slip rupture and a deep buried circular crack are $2/\pi$ and $7\pi/8$, respectively

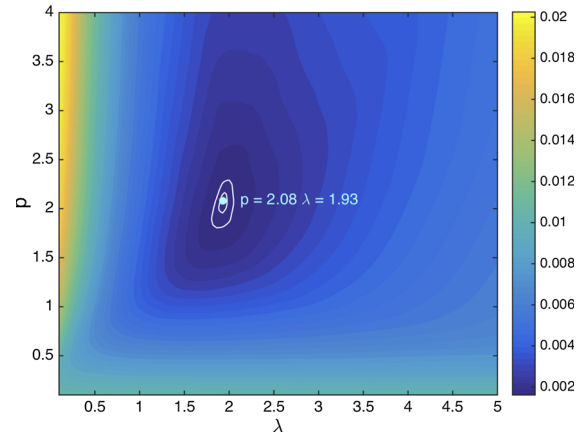

Figure 9
Misfit between moment-area data from our rate-and-state catalog and our Eq. (8) as a function of λ and p. The best fitting values are $p = 2.08$ and $\lambda = 1.93$ (*light blue dot*). White contours are the 95% and 99% confidence levels

C due to the free surface, which we refer to as 'C effect' hereafter (Fig. 8). When a rupture grows towards the free surface (L/W_s increases and approaches 1 in Fig. 8), C decreases rapidly by approximately a factor of 2. The C values of a deep buried circular crack and an infinitely long strike-slip rupture that reaches the surface are $C_0 = 7\pi/8$ and $C_1 = 2/\pi$, respectively (Kanamori and Anderson 1975), which differ by a factor of about 4. Equation (7) shows that the decrease of C pushes Stage 3 'to the right' in the M_0–A plot (larger moment for a given area). This effectively increases the apparent value of the scaling exponent n and extends the range of Stage 2. In nature, the C effect always occurs together with the G effect and both contribute to Stage 2. Thus the transition between small buried ruptures and large surface-breaking ruptures is the major origin of Stage 2. The combination of C effect and G effect, that we name 'surface rupture effect', are sufficient to explain the observed Stage 2 in both real world earthquakes and simulated earthquakes.

Our crack model fits quantitatively well with both empirical and simulation M_0–A data. However, there is no analytical expression for crack models. Here we propose a simplified equation in closed form for the shape factor C that can be useful for practical purposes (Fig. 8)

$$C\left(\frac{L}{W_s}\right) = C_0 + \frac{C_1 - C_0}{1 + (\lambda W_s/L)^p}. \qquad (8)$$

This equation has the following controlling parameters: the seismogenic depth W_s (or, in more general terms, the maximum rupture width) and two tunable variables p and λ. Similar to Eq. (4) we get the following general forms of the M_0–A relation

$$M_0 = A^{3/2} \times \frac{\overline{\Delta\tau}}{C} \quad L \le W_s, \qquad (9a)$$

$$M_0 = A \times W_s \times \frac{\overline{\Delta\tau}}{C} \quad L > W_s. \qquad (9b)$$

We performed a grid search to find the values of parameters p and λ that minimize the least squares misfit between the moment—area data from rate-and-state simulations (smoothed by a sliding median) and predicted by combining Eqs. (8) and (9a, b). We find that the best fitting values and their 95% confidence intervals are $p = 2.08 \pm 0.2$ and $\lambda = 1.93 \pm 0.1$ (Fig. 9).

Combining Eqs. (8) and (9) gives a convenient and reasonably accurate relation between seismic moments and rupture area across all earthquake magnitudes. The M_0–A relation resulting from Eq. (8) with the best fitting parameter values p and λ is presented in black in (Fig. 7). It is in very good

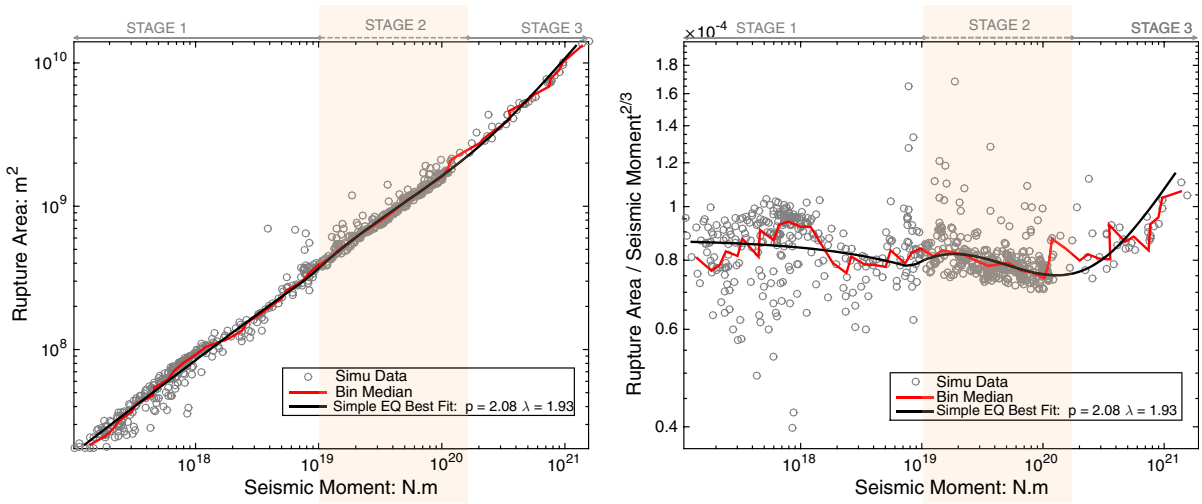

Figure 10

Left earthquake M_0–A scaling in synthetic catalogs and best fitting simple practical model. *Right* reduced M_0–$A/M_0^{2/3}$ scaling, which allows a more critical assessment of the agreement between Eq. (8) and the synthetic rate-and-sate catalog. *Grey circles* synthetic earthquake data from our rate-and-state simulation. *Red curve* sliding median of synthetic data. *Black curve* proposed simple Eq. (8) with best fitting parameters $p = 2.08$ and $\lambda = 1.93$. The proposed equation is in good agreement with the synthetic data

agreement with both rate-and-state simulation results and the earthquake data and is noticeably better than the original crack model, especially in Stage 2. Plotting M_0 vs. $A/M_0^{2/3}$ (Fig. 10) allows a more critical assessment of the agreement between Eq. (8) and the synthetic rate-and-sate catalog.

Equation (8) is simple and has a clear physically meaning. Its asymptotic limits, C_0 and C_1, are consistent with values from well-accepted crack models. The value of λ is expected to be 2 from the free surface effect in the absence of deep rupture penetration, and the best fitting value $\lambda = 1.93$ indicates that no deep penetration is required by our model. In comparison, fitting our rate-and-state catalog with Shaw's model requires rupture to extend much deeper, 200% of the seismogenic depth. Most importantly, our physically sound model fits very well the real earthquake data, so it can be used as a simple yet accurate moment-area scaling model. Adopting the values $p = 2$ and $\lambda = 2$, within the 95% confidence level of the best fitting values, we propose the following simple equation for use in practical applications:

$$C\left(\frac{L}{W_s}\right) = \frac{\pi}{8}\left(7 - \frac{3}{1 + (2W_s/L)^2}\right). \qquad (10)$$

5. Conclusion

We investigated the mechanical origin of the transition in earthquake moment-area scaling between the small (self-similar) and very large (W-model) earthquake scaling regimes via rate-and-state earthquake cycle simulations, analytical dislocation models and numerical crack models on strike-slip faults. We demonstrated that the counter-intuitive form of the transitional Stage 2 (M_0–A^2) can be mainly attributed to surface rupture effects, comprising an effective rupture elongation along-dip due to a mirror effect (G effect) and systematic changes of the shape factor relating slip to stress drop (C effect). Other effects, like deep rupture penetration, deeper viscous layer and scale-dependency of stress drop, while possibly present and contributing to the origin of the 3-stage model, should be considered as secondary. Based on this physical insight, we proposed a physically sound approximate formula that conveniently relates seismic moment and rupture size across all earthquake magnitudes, and can be of practical use in earthquake hazard assessment and ground motion prediction. The parameters of our rate-and-state model (seismogenic depth and stress drop) and of our simplified equation are calibrated to

fit the empirical 3-stage model. While our models require a seismogenic depth of 20 km, in the upper end of typical values for strike-slip faults, including additional mechanisms like scale-dependency of stress drop might allow us to fit the real earthquake data with a smaller seismogenic depth.

Acknowledgements

This study was based on the 2015 research project 'Improvement for uncertainty of strong ground motion prediction' by the Nuclear Regulation Authority (NRA), Japan.

References

Dalguer, L. A., Miyake, H., Day, S. M., & Irikura, K. (2008). Surface rupturing and buried dynamic rupture models calibrated with statistical observations of past earthquakes. *Bulletin of the Seismological Society of America, 98,* 1147–1161. doi:10.1785/0120070134.

Fujii, Y., & Matsu'ura, M. (2000). Regional difference in scaling laws for large earthquakes and its tectonic implication. *Pure and Applied Geophysics, 157*(11–12), 2283–2301.

Gallovič, F. (2008). Heterogeneous Coulomb stress perturbation during earthquake cycles in a 3D rate-and-state fault model. *Geophysical Research Letters*, *35*(21).

Hanks, T. C., & Bakun, W. H. (2002). A bilinear source-scaling model for *M*–log *A* observations of continental earthquakes. *Bulletin of the Seismological Society of America, 92*(5), 1841–1846.

Hanks, T. C., & Bakun, W. H. (2014). *M*–log *A* models and other curiosities. *Bulletin of the Seismological Society of America, 104*(5), 2604–2610.

Hillers, G., Ben-Zion, Y., & Mai, P. M. (2006). Seismicity on a fault controlled by rate-and-state dependent friction with spatial variations of the critical slip distance. *Journal of Geophysical Research: Solid Earth, 111*(B1), B01403.

Hillers, G., Mai, P. M., Ben-Zion, Y., & Ampuero, J. P. (2007). Statistical properties of seismicity of fault zones at different evolutionary stages. *Geophysical Journal International, 169*(2), 515–533.

Irikura, K., & Miyake, H. (2001). Prediction of strong ground motions for scenario earthquakes. *Journal of Geography (Chigaku Zasshi), 110*(6), 849–875.

Irikura, K., & Miyake, H. (2011). Recipe for predicting strong ground motion from crustal earthquake scenarios. *Pure and Applied Geophysics, 168*(1–2), 85–104.

Kanamori, H., & Anderson, D. L. (1975). Theoretical basis of some empirical relations in seismology. *Bulletin of the Seismological Society of America, 65*(5), 1073–1095.

Leonard, M. (2010). Earthquake fault scaling: Self-consistent relating of rupture length, width, average displacement, and moment release. *Bulletin of the Seismological Society of America, 100*(5A), 1971–1988.

Marone, C. (1998). Laboratory-derived friction laws and their application to seismic faulting. *Annual Review of Earth and Planetary Sciences, 26*(1), 643–696.

Matsu'ura, M., & Sato, T. (1997). Loading mechanism and scaling relations of large interplate earthquakes. *Tectonophysics, 277*(1), 189–198.

Miyakoshi, K., Irikura, K., & Kamae, K. (2015). Re-examination of scaling relationships of source parameters of the inland crustal earthquakes in Japan based on the waveform inversion of strong motion data. *Journal of Japan Association for Earthquake Engineering, 15–7,* 141–156. **(in Japanese with English abstract)**.

Murotani, S., Matsushima, S., Azuma, T., Irikura, K., & Kitagawa, S. (2015). Scaling relations of source parameters of earthquakes occurring on inland crustal mega-fault systems. *Pure and Applied Geophysics, 172*(5), 1371–1381.

Okada, Y. (1992). Internal deformation due to shear and tensile faults in a half-space. *Bulletin of the Seismological Society of America, 82*(2), 1018–1040.

Romanowicz, B., & Rundle, J. B. (1993). On scaling relations for large earthquakes. *Bulletin of the Seismological Society of America, 83*(4), 1294–1297.

Rubin, A. M., & Ampuero, J. P. (2005). Earthquake nucleation on (aging) rate and state faults. *Journal of Geophysical Research: Solid Earth, 110*(B11), B11312.

Scholz, C. H. (1982). Scaling laws for large earthquakes: consequences for physical models. *Bulletin of the Seismological Society of America, 72*(1), 1–14.

Scholz, C. H. (1998). Earthquakes and friction laws. *Nature, 391*(6662), 37–42.

Shaw, B. E. (2009). Constant stress drop from small to great earthquakes in magnitude-area scaling. *Bulletin of the Seismological Society of America, 99*(2A), 871–875.

Shaw, B. E., & Wesnousky, S. G. (2008). Slip-length scaling in large earthquakes: The role of deep-penetrating slip below the seismogenic layer. *Bulletin of the Seismological Society of America, 98*(4), 1633–1641.

Somerville, P., Irikura, K., Graves, R., Sawada, S., Wald, D., Abrahamson, N., et al. (1999). Characterizing crustal earthquake slip models for the prediction of strong ground motion. *Seismological Research Letters, 70*(1), 59–80.

Song, S. G., Beroza, G. C., & Segall, P. (2008). A unified source model for the 1906 San Francisco earthquake. *Bulletin of the Seismological Society of America, 98*(2), 823–831.

Streit, J. E., & Cox, S. F. (2001). Fluid pressures at hypocenters of moderate to large earthquakes. *Journal of Geophysical Research: Solid Earth, 106*(B2), 2235–2243.

Wells, D. L., & Coppersmith, K. J. (1994). New empirical relationships among magnitude, rupture length, rupture width, rupture area, and surface displacement. *Bulletin of the Seismological Society of America, 84*(4), 974–1002.

Bodin, P., & Brune, J. N. (1996). On the scaling of slip with rupture length for shallow strike-slip earthquakes: Quasi-static models

and dynamic rupture propagation. *Bulletin of the Seismological Society of America, 86*(5), 1292–1299.

Mai, P. M., & Beroza, G. C. (2000). Source scaling properties from finite-fault-rupture models. *Bulletin of the Seismological Society of America, 90*(3), 604–615.

Causse, M., & Song, S. G. (2015). Are stress drop and rupture velocity of earthquakes independent? Insight from observed ground motion variability. *Geophysical Research Letters, 42*(18), 7383–7389.

(Received August 1, 2016, revised December 13, 2016, accepted January 2, 2017, Published online January 25, 2017)